Non-equilibrium impurity treatment for JOREK Disruption Mitigation simulations

A particle-based model

Di Hu (胡地, hudi2@buaa.edu.cn)
Collaborators: G.T.A. Huijsmans, E. Nardon, M. Hoelzl, M. Lehnen, D. Bonfiglio & JOREK team.

School of Physics, Beihang University
No. 37 Xueyuan Road, Haidian District, Beijing, China, 100083.

EUROfusion DE LA RECHERCHE À L'INDUSTRIE cea Remote iter china eu india japan korea russia usa

IPP Max-Planck-Institut für Plasmaphysik 北京航空航天大學 BEIHANG UNIVERSITY TU/e EINDHOVEN UNIVERSITY OF TECHNOLOGY CONSORZIO RFX Ricerca Formazione Innovazione

Contents

The Massive Material Injection simulations

- Massive Material Injection (MMI) is essential for Disruption Mitigation System (DMS) in future high performance tokamaks such as ITER.
- Massive Gas Injection (MGI), Shattered Pellet Injection (SPI), Dispersive Shell Pellet Injection (DSPI) etc..
- Numerical simulations provides insight into the asymmetry of radiation power density as well as the interplay between the MHD modes and the injected materials.

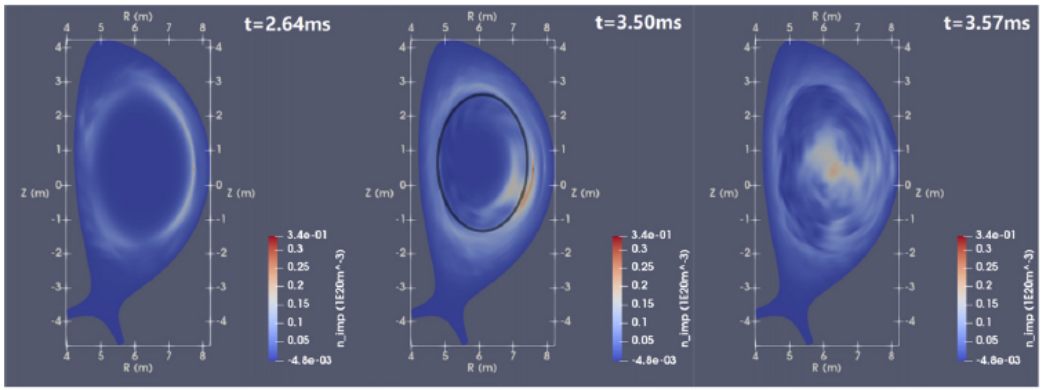

D. Hu et al., Nucl. Fusion 61 (2021) 026015

The non-equilibrium impurities

- JOREK has been assuming Coronal Equilibrium (CE) distribution of the impurity charge state distribution in the past MMI simulations.
- However, deviation from CE could occur in the early phase of injection if the cooling is not fast enough.

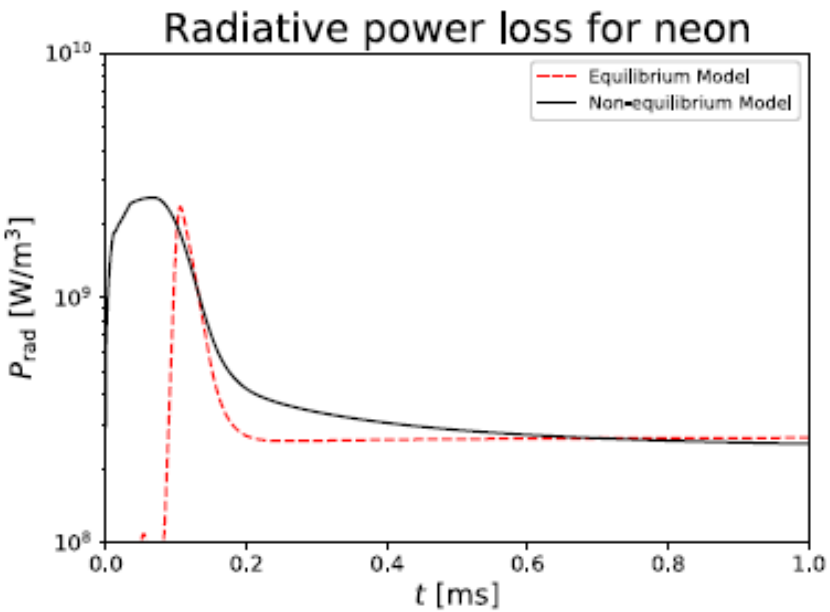

(a)

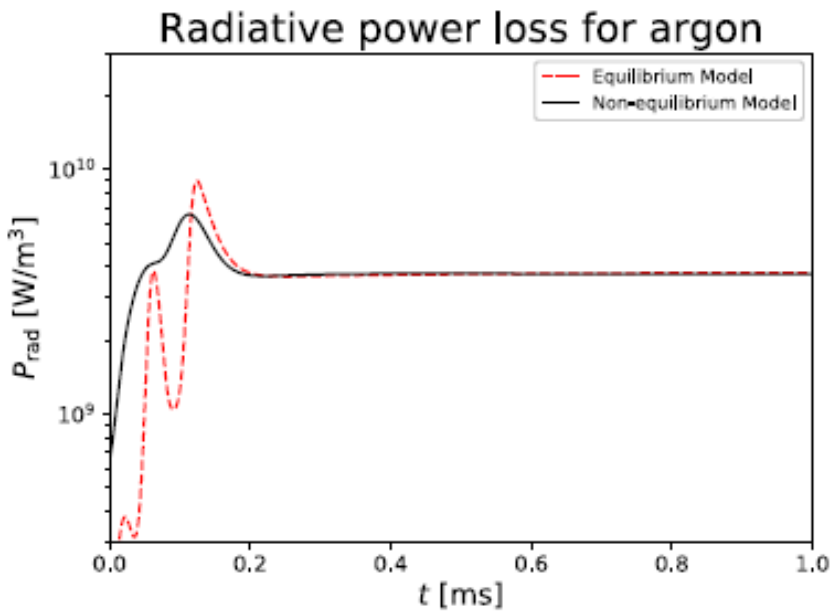

(b)

D. Hu et al., Nucl. Fusion 61 (2021) 026015

Particle based non-equilibrium impurity modelling

- To capture the self-consistent evolution of the impurity charge state distribution, one way is to model each charge state (of several bundles of them) as separate fluid.
- We hereby develop another approach by modelling the impurities as "marker-particles" flowing along the fluid velocity field lines, ionizing and recombining independently according to local electron temperature and density.
- The particles are pushed for several time steps within a given fluid field in-between the fluid time steps.
- The resulting charge state distribution, as well as the ionization power and radiation power density are projected onto the fluid field for fluid time-stepping.
- Comparison against CE impurity fluid model and benchmark against previous non-equilibrium impurity NIMROD and M3D-C1 simulations are carried out.

The marker-particle pusher

- The super-particles are not pushed according to their respective Newton's law.
- In the reduced MHD, the magnetic and the velocity field could be written as

$$\mathbf{B} = F_0 \nabla\phi + \nabla\psi \times \nabla\phi, \tag{1}$$

$$\mathbf{v} = v_{\parallel}\mathbf{B} - R^2 \nabla u \times \nabla\phi. \tag{2}$$

- The velocity then has the following expression:

$$\mathbf{v} = \left(-R\partial_Z u + \frac{v_{\parallel}}{R}\partial_Z\psi\right)\mathbf{e}_R + \left(R\partial_R u - \frac{v_{\parallel}}{R}\partial_R\psi\right)\mathbf{e}_Z + \frac{F_0}{R}v_{\parallel}\mathbf{e}_\phi. \tag{3}$$

- The "marker-particles" are pushed along the velocity field line with the local fluid velocity.
- New super-particles are generated according to reject-sampling of the impurity density source after each fluid time step.

Ionization, recombination

- Due to the marker-particle pusher, it is possible to assign a charge state distribution instead of a single charge to each super-particle.
- This is favorable for the smoothness of ionization/recombination under MMI consideration, avoiding cancellation of large terms.
- The ionization, the recombination and the radiation are determined by both the local fluid electron density, temperature and open ADAS atomic data.
- The charge state distribution evolution for each super-particle is:

$$\frac{df_i}{dt} = n_e \left[S_{i-1}(T_e) f_{i-1} - \left(S_i(T_e) f_i + \alpha_i(T_e) \right) f_i + \alpha_{i+1} f_{i+1} \right]. \qquad (4)$$

- Here, S_i and α_i are the ionization rate and recombination rate of charge state i respectively, while f_i is the number density of that charge state, and n_e is the electron density.

Ionization energy moment projection

- Five particle moments are projected back to the fluid for time stepping.
- Details of projection in D.C. van Vugt et al., Phys. Plasmas **26**, 042508 (2019);
- The first is the ionization power density, which is representing the energy taken from the electron thermal energy to compensate the impurity's ionization energy.

$$\Delta E_{ion} = n_e \Delta t \sum_{i=0}^{Z-1} \left(N_{imp}^{i+} S_i(T_e) - N_{imp}^{i+1+} \alpha_i(T_e) \right) E_{ion}^{i+}. \tag{5}$$

- In reality, the part of ionization potential energy would be lost at the time of recombination through recombination radiation in the absence of three-body recombination.
- In open ADAS data, it's not trivial to separate the recombination radiation from the total continuum radiation. Thus we simply feed the ionization energy back to the plasma to avoid double counting.

Radiation power moment projection

- The second is the radiation power density. With a given charge state distribution for a given super-particle, the total radiation power P_{rad} is then a function of the electron density and temperature

$$\begin{aligned} P_{rad} &= n_e n_{imp} L_{rad}(n_e, T_e) \\ &= n_e \sum_{i=0}^{Z} n_{imp}^{i+} \left(L_L^{i+}(n_e, T_e) + L_R^{i+}(n_e, T_e) + L_B^{i+}(n_e, T_e) \right) \end{aligned} \quad (6)$$

- Here, n_{imp} is the total density of the impurity species, while n_{imp}^{i+} is that of each charge state. The radiation power function L_L^{i+}, L_R^{i+} and L_B^{i+} are the line radiation, the recombination radiation and the bremsstrahlung radiation of each charge state respectively.
- The radiation power functions are also obtained from the open ADAS database.

Charge state information and density

- We need the effective charge of the impurity species as well as the mean charge for the resistivity calculation and the electron density calculation. The last projection is the total impurity number density.
- The effective charge of the impurity is defined as:

$$Z_{eff} \equiv \frac{\sum_i n_i Z_i^2}{\sum_i n_i Z_i}.$$

- This is use in the calculation of the Spitzer-like resistivity

$$\eta = Z_{eff} \frac{\eta_0}{\max\left(T_e, T_{thres}\right)^{3/2}} \times \frac{1 + 1.198\, Z_{eff} + 0.222\, Z_{eff}^2}{1 + 2.966\, Z_{eff} + 0.753\, Z_{eff}^2}. \tag{7}$$

- The mean charge is simply

$$Z_{imp} \equiv \frac{\sum_i n_i Z_i}{\sum_i n_i}. \tag{8}$$

The initial equilibrium

- Same DIII-D equilibrium with B.C. Lyons, C.C. Kim, Y.Q. Liu, Plasma Phys. Control. Fusion **61**, 064001 (2019).
- The equilibrium corresponds to the DIII-D shot 137611 at 1950ms.
- The initial plasma consists of pure deuterium.
- All runs are axisymmetric.

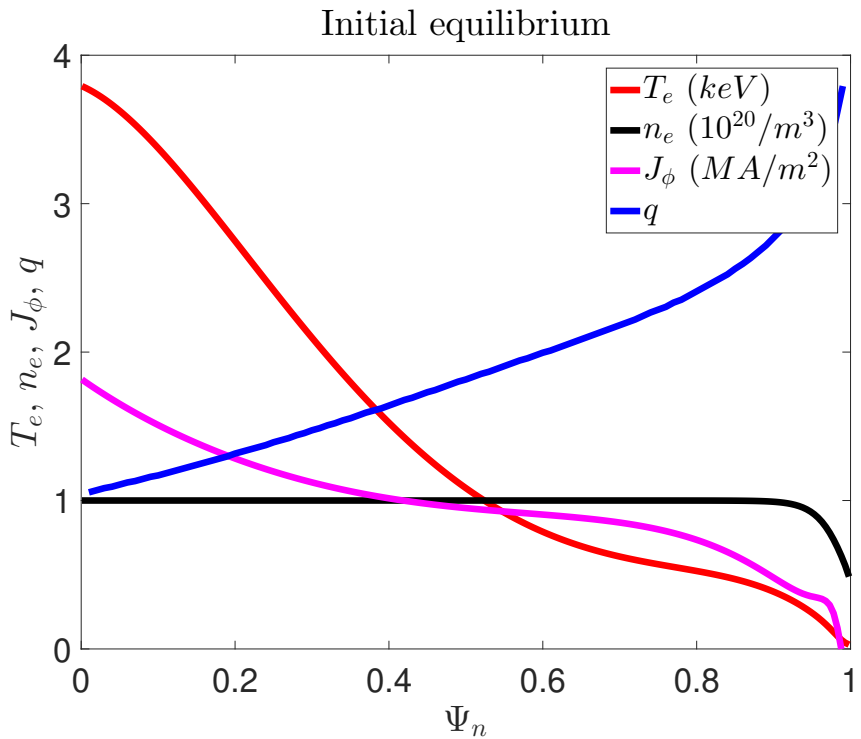

The transport parameters

- We use the same diffusivities with previous NIMROD and M3D-C1 simulations.
- We use the isotropic density diffusivity $D = 10m^2/s$, and the perpendicular thermal diffusivity is set to $100m^2/s$.
- The parallel thermal diffusivity is set to $10^8 m^2/s$. For the two temperature case, the same heat conduction is used for both electrons and ions.
- The viscosity corresponds to a momentum diffusivity of $100m^2/s$ initially, but with the same temperature dependence of the resistivity so that the magnetic Prandtl number is constant, as opposed to the NIMROD & M3D-C1 cases where the momentum diffusivity is constant.
- We use two different kinds of resistivity models, namely the constant resistivity and the Spitzer-like resistivity. For the constant resistivity, the resistivity is fixed to $10^{-5}\Omega m$. For the Spitzer-like resistivity, η_0 is set to $1.83339 \times 10^{-8}\Omega m$.

The injection source

- We use a Gaussian shape distribution for our impurity density source with the following shape:

$$S_n \propto \exp\left(-\frac{(R-R_f)^2+(Z-Z_f)^2}{\Delta r_{NG}^2}\right) \times \exp\left(-\left(\frac{\phi-\phi_f}{\Delta\phi_{NG}}\right)^2\right). \quad (9)$$

- In this axisymmetric simulation, we simply set $\Delta\phi_{NG}$ to be a very large number, and we set $\Delta r_{NG}^2 = 0.356m$, $R_0 = 1.77037m$ and $Z_0 = 0.01447m$ so that we have generally the same deposition shape with previous NIMROD and M3D-C1 simulations.
- The volume integrated impurity atom injection rate is approximately 4.37×10^{23} per second, the same with previous NIMROD and M3D-C1 simulations.

Comparison between CE and non-equilibrium impurities

- Stronger ionization power for the CE treatment due to impurities jumping to the equilibrium charge states.
- In general, the CE treatment shows delayed rise in the total cooling power, as well as in other characteristic events.
- Comparable peak level.
- Two temperature model behaves better.

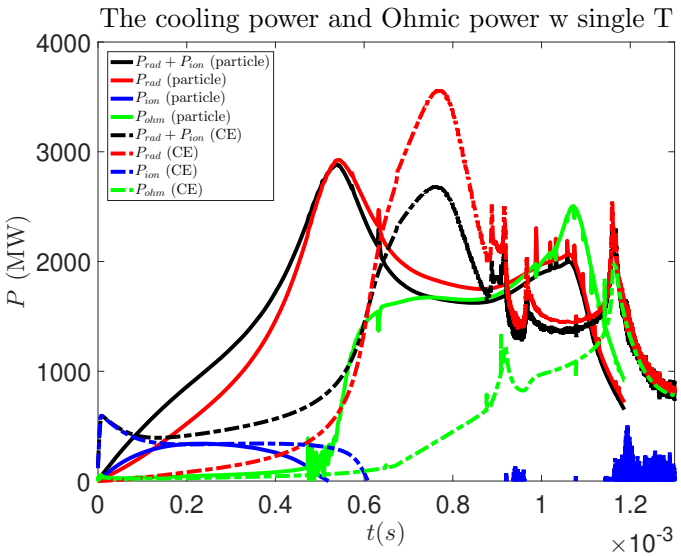

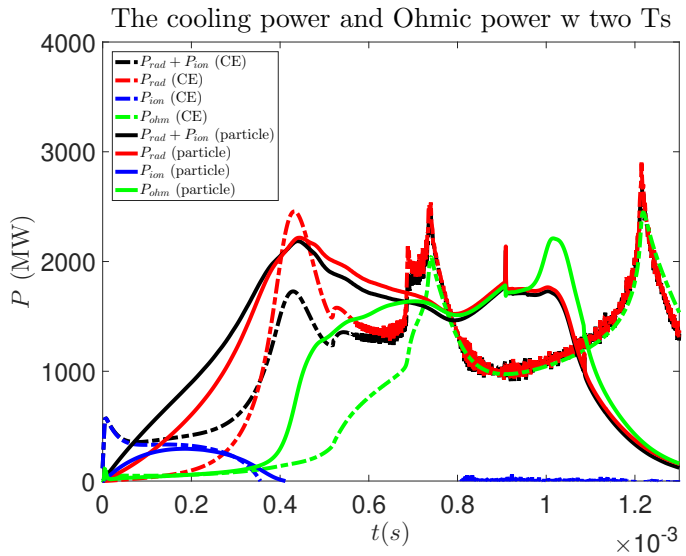

Two temperature argon mean charge comparison

The mean impurity charge for the non-equilibrium treatment at time (a) $t = 0.26ms$, (b) $t = 0.45ms$ and (c) $t = 0.78ms$.

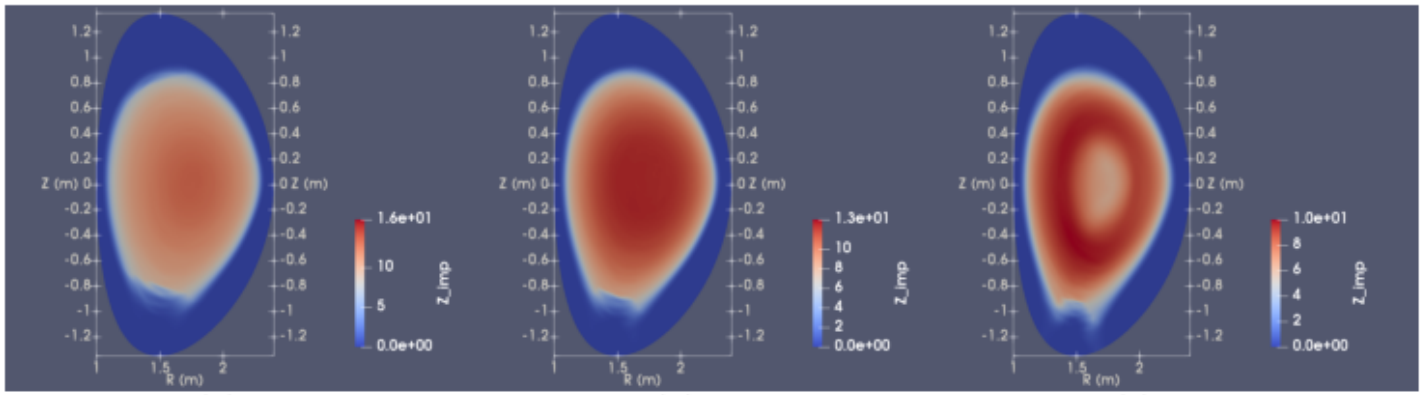

(a) (b) (c)

(d) (e) (f)

Comparison between temperature models

- The two temperature model shows lesser cooling peak for the argon case, but comparable plateau value.
- The single temperature model exhibits delay compared with the two temperature model.
- The balance between the Ohmic heating and the cooling power occurs at the plateau stage.

The cooling power and ohmic heating for Ar injection

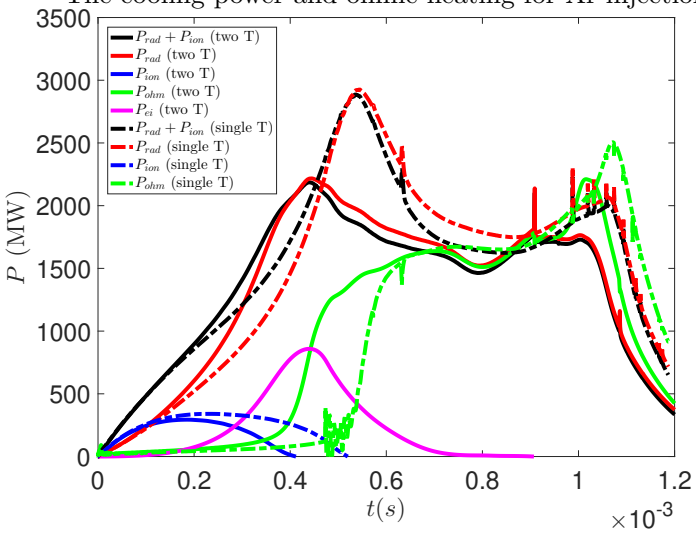

The cooling power and ohmic heating for Ne injection

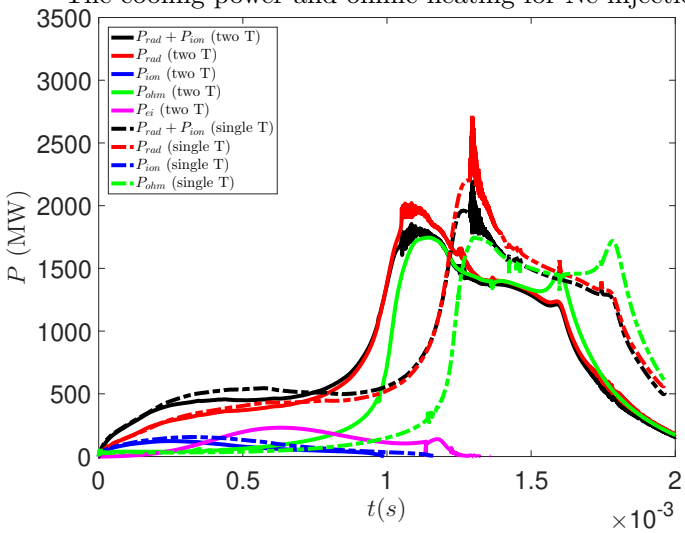

Thermal energy evolution

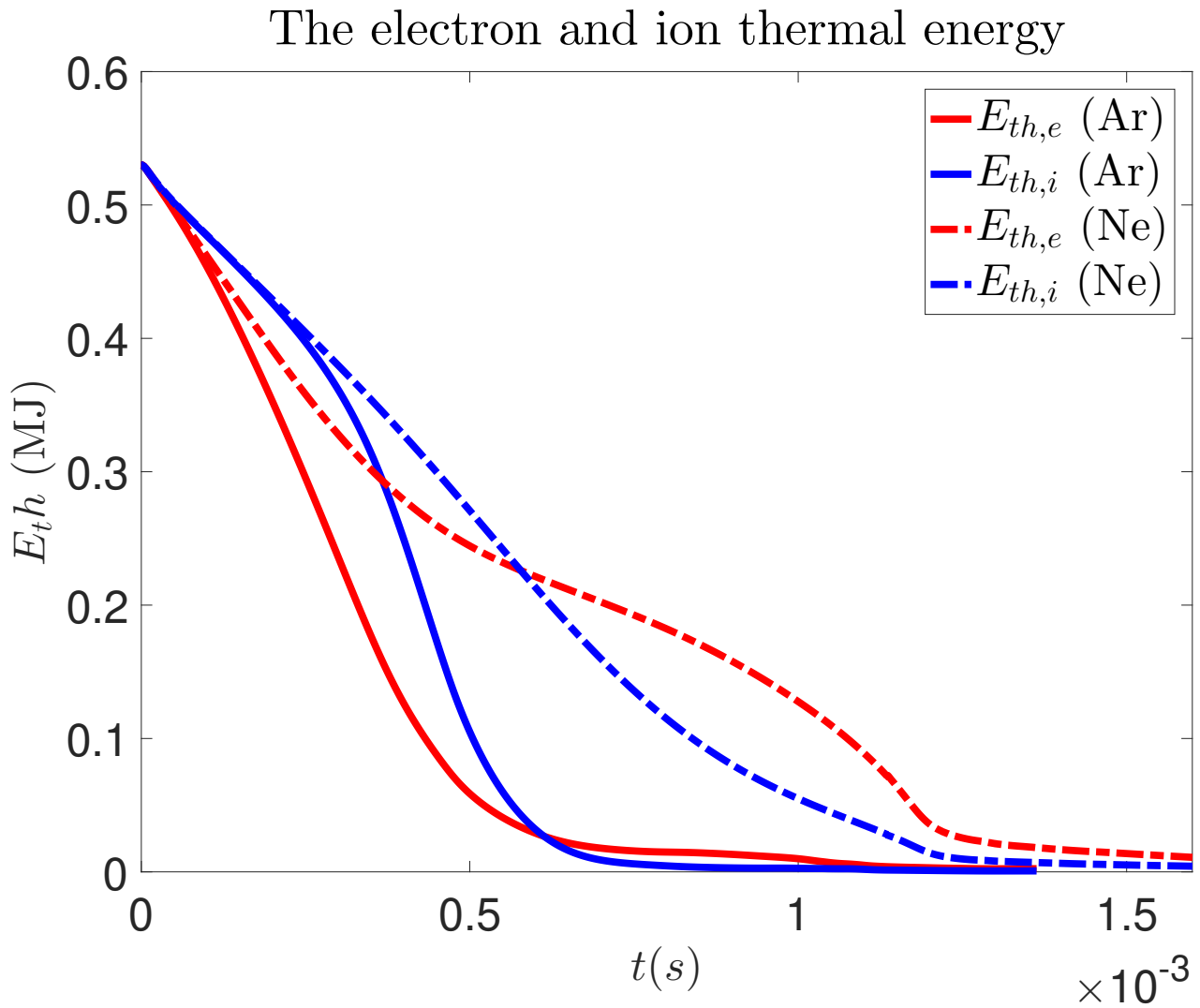

The charge state evolution

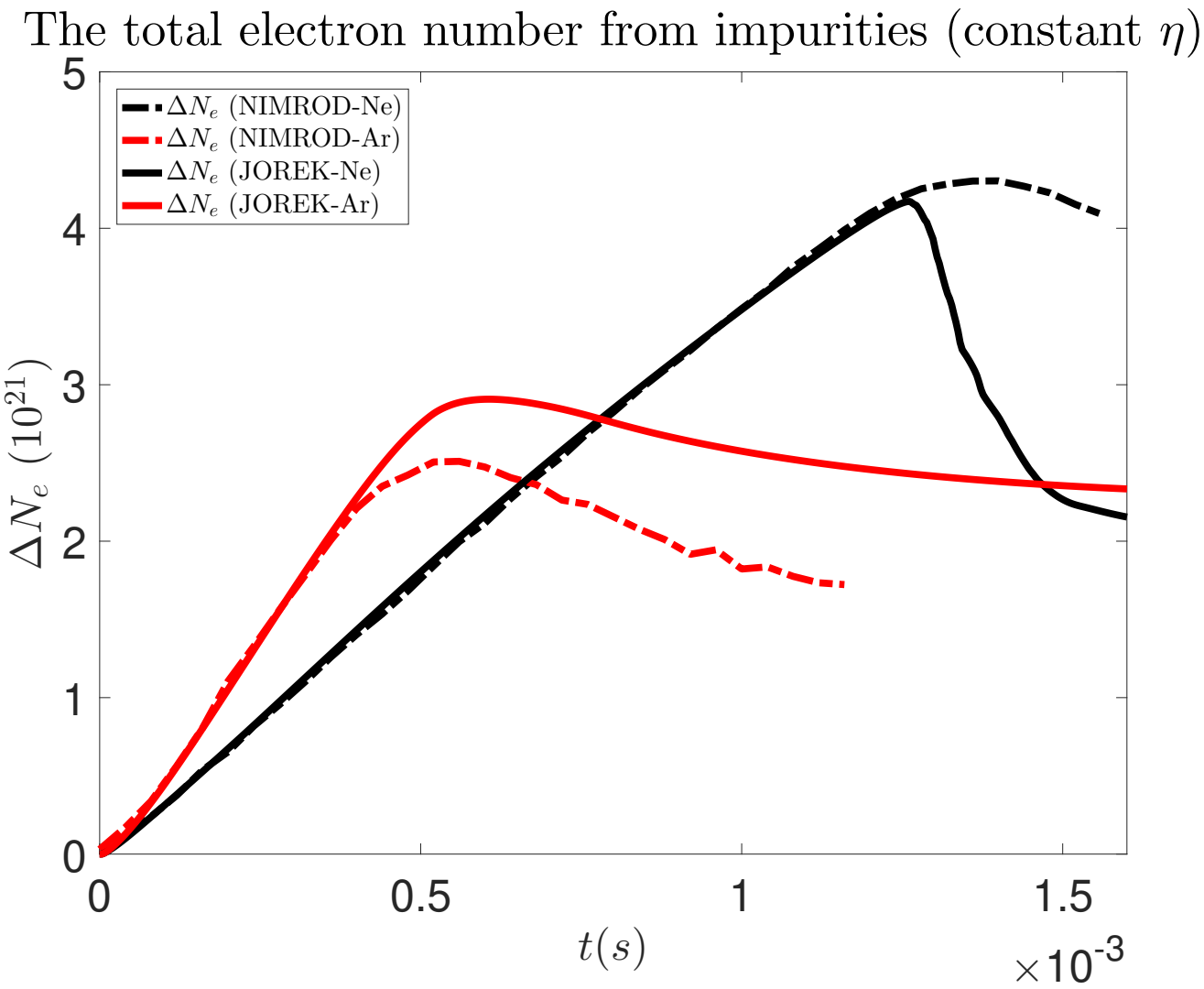

Evolution of integrated quantities

- Despite the difference in the atomic data, generally good agreement is found for both cases.
- Same peak level and termination time for the argon case. General agreement for the neon case apart from some deviation near the plasma termination.
- The neon case deviation is likely due to the deviation in the recombination rate.

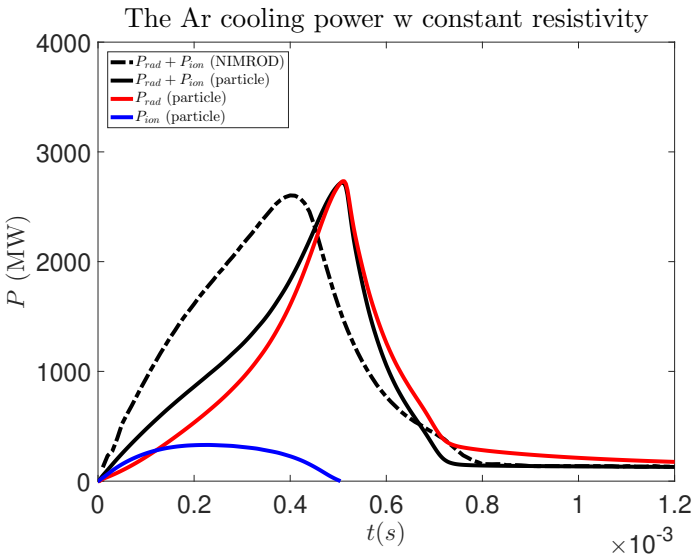

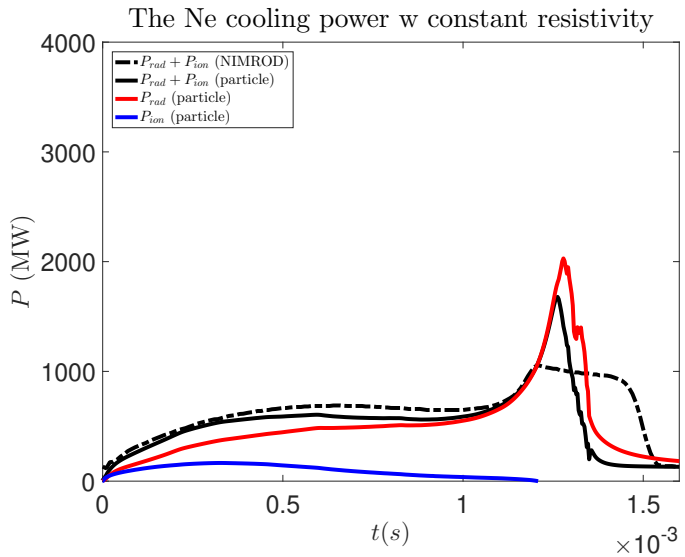

The charge state evolution

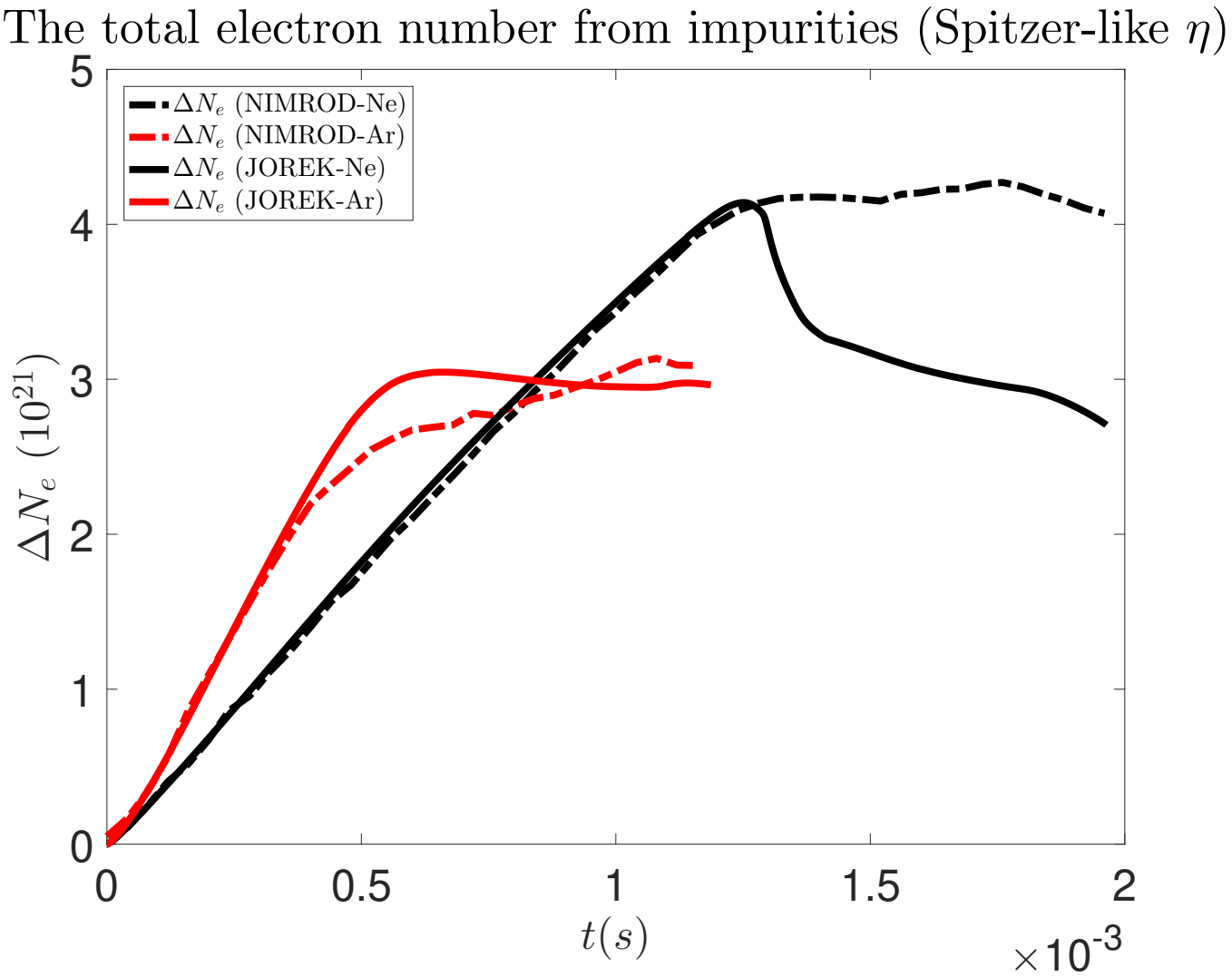

Evolution of integrated quantities

- Despite the difference in the atomic data, generally good agreement is found for both cases.
- Same peak level and termination time for the argon case. General agreement for the neon case apart from some deviation near the plasma termination.
- The neon case deviation is likely due to the deviation in the recombination rate.

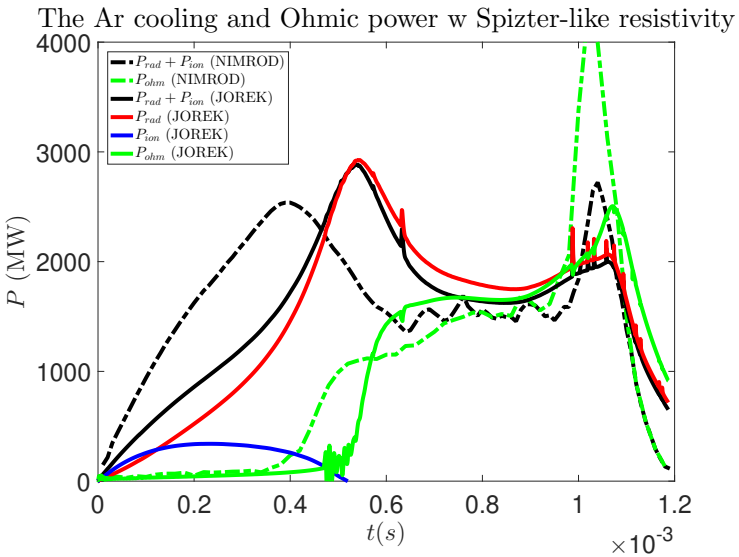

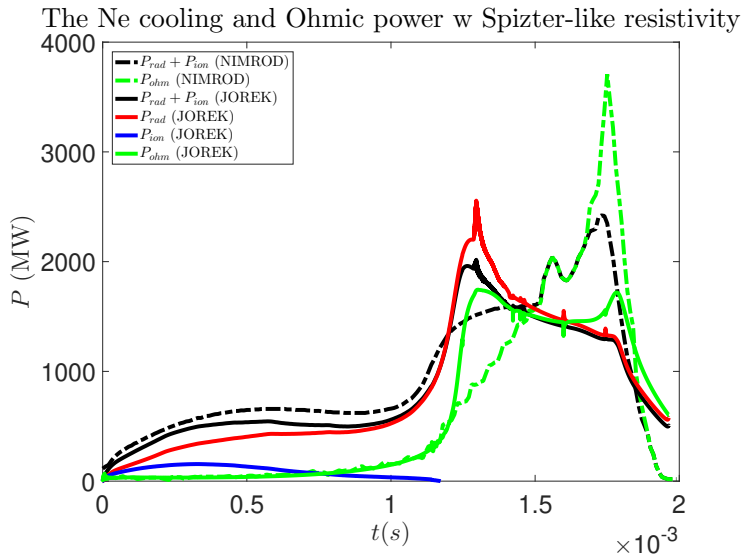

2D T_e profile comparison

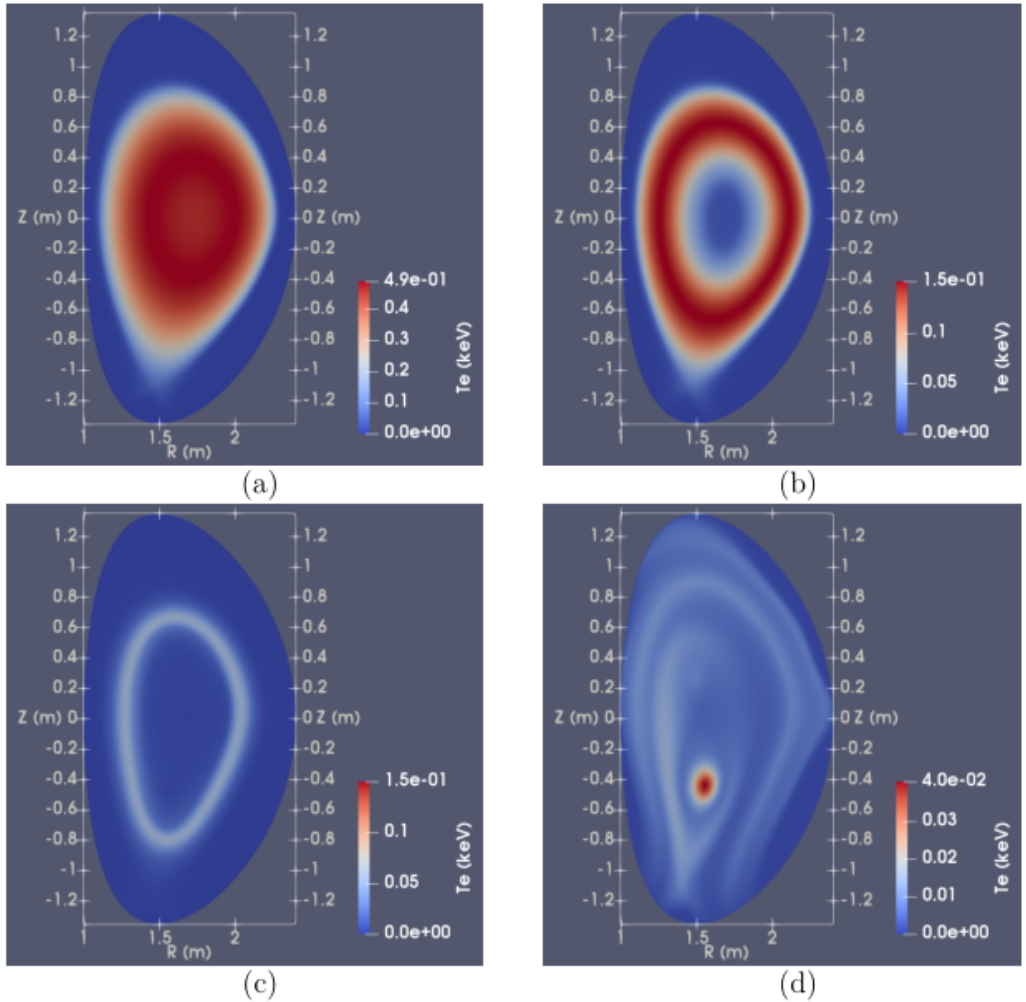

2D T_e profile comparison

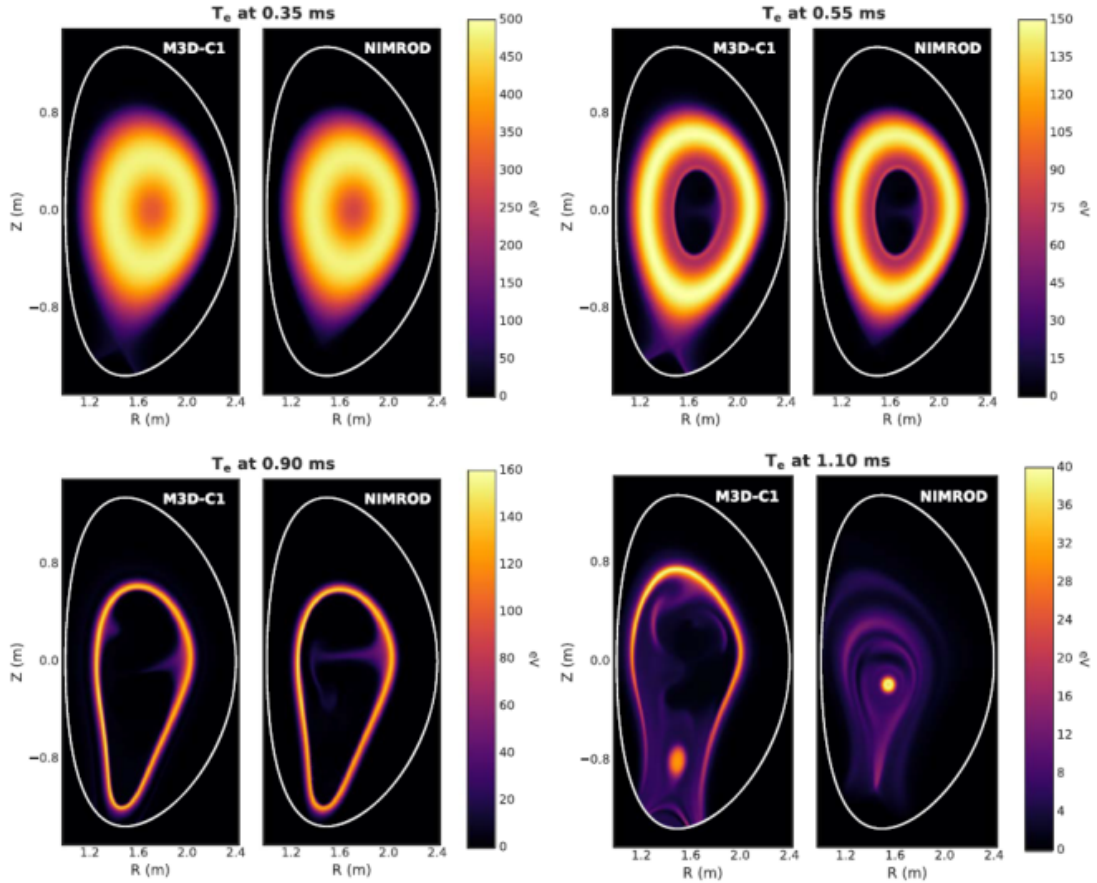

B.C. Lyons, C.C. Kim, Y.Q. Liu, Plasma Phys. Control. Fusion 61, 064001 (2019)

2D J_ϕ profile comparison

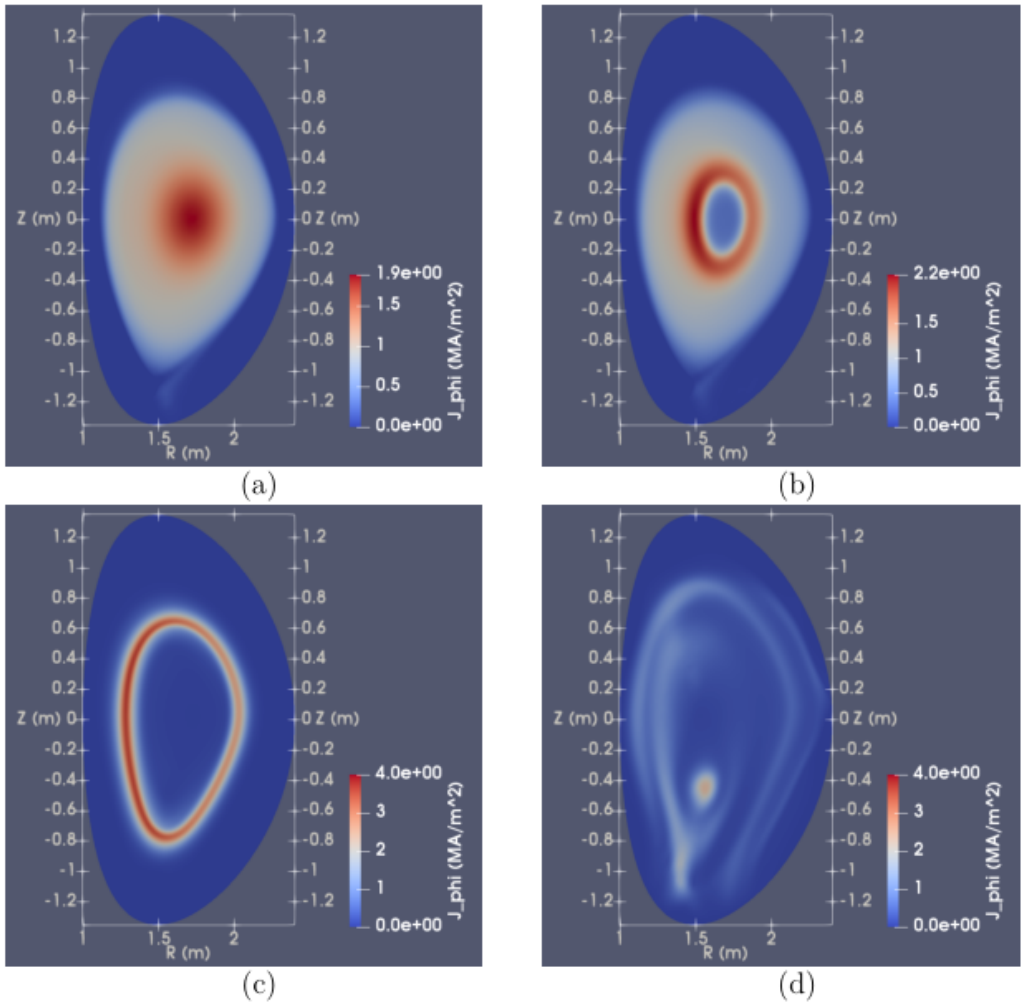

2D J_ϕ profile comparison

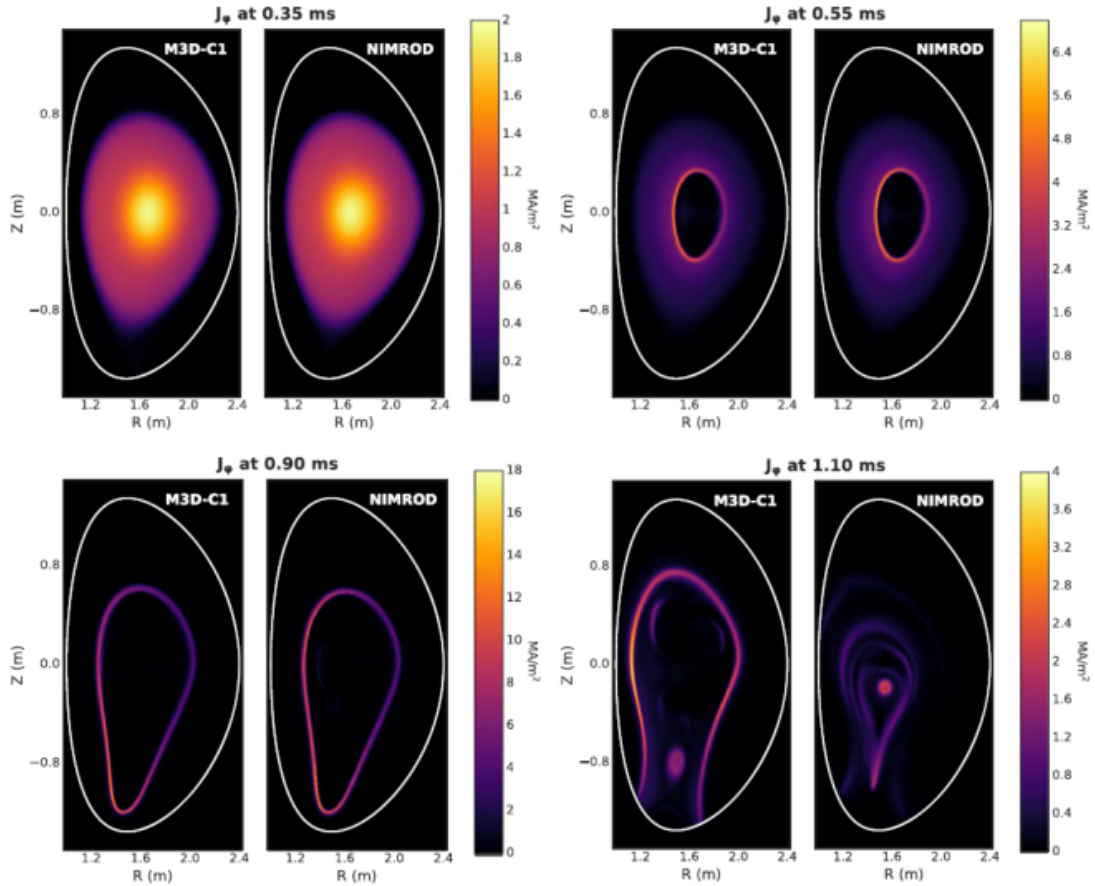

B.C. Lyons, C.C. Kim, Y.Q. Liu, Plasma Phys. Control. Fusion 61, 064001

Conclusion

- Particle-based non-equilibrium impurity treatment implemented using open-ADAS data.
- Super-particles are generated by reject-sampling according to impurity density source, pushed along the fluid velocity field line while ionizing/recombining independently. The particle moments are projected for fluid time-stepping.
- Compared with the CE result, the non-equilibrium result captured the early radiative cooling.
- The peak cooling power and Ohmic power are comparable between the CE and the non-equilibrium treatment.
- The CE treatment show delay of characteristic events due to failure in capturing early phase cooling.
- The charge state evolution lags behind the evolution of the CE charge state distribution as would be expected.

Conclusion

- Benchmark with previous NIMROD and M3D-C1 cases show general agreement despite the difference in the atomic data, highlighting the robustness of the radiative collapse dynamic.
- The peak level of the cooling power and the Ohmic power are comparable between the codes.
- The integrated quantities show the same characteristic behavior, as well as similar timing.
- The 2D profile evolution show good agreement between the codes.
- The JOREK non-equilibrium impurity model is now ready for production, compatible with both single and two temperature model.
- Diffusive particle movement may need to be added to the particle pusher for scenarios where diffusive process dominate over the convective process.

Acknowledgement

- This work has been carried out within the framework of the EUROfusion Consortium and has received funding from the Euratom research and training program 2014-2018 and 2019-2020 under grant agreement No 633053. The views and opinions expressed herein do not necessarily reflect those of the European Commission.
- Part of this work is supported by the National Natural Science Foundation of China under Grant No. 11905004, and the National MCF Energy R&D Program of China under Grant No. 2019YFE03010001.
- This work has been co-funded by the ITER Organization under the implementing agreement IO/IA/19/4300002026. ITER is the Nuclear Facility INB no. 174. The views and opinions expressed herein do not necessarily reflect those of the ITER Organization. This publication is provided for scientific purposes only. Its contents should not be considered as commitments from the ITER Organization as a nuclear operator in the frame of the licensing process.

Backup Slides

The governing equations

- First, we have the induction equation:

$$\frac{\partial \psi}{\partial t} = \eta(T_e)\Delta^*\psi - R\{u,\psi\} - F_0\frac{\partial u}{\partial \phi}, \tag{10}$$

$$j = \Delta^*\psi, \quad j_\phi = -j/R, \tag{11}$$

  with Poisson bracket $\{f,g\} \equiv R(\nabla f \times \nabla g)\cdot\nabla\phi$.
- Second, the continuity equation for both the total plasma mass density and that for the impurity species is not affected:

$$\frac{\partial \rho}{\partial t} = -\nabla\cdot(\rho\mathbf{v}) + \nabla\cdot(D\nabla\rho) + S_{bg} + S_{imp}, \tag{12}$$

$$\frac{\partial \rho_{imp}}{\partial t} = -\nabla\cdot(\rho_{imp}\mathbf{v}) + \nabla\cdot(D\nabla\rho_{imp}) + S_{imp}. \tag{13}$$

  Here, the impurity density source S_{imp} determines the particle generation by reject-sampling.

The governing equations

Third, we have the perpendicular and the parallel momentum equations:

$$\begin{aligned} R\nabla\cdot\left[R^2\frac{\partial}{\partial t}\left(\rho\nabla_{pol}u\right)\right] &= \frac{1}{2}\left\{R^2\left|\nabla_{pol}u\right|^2, R^2\rho\right\}+\left\{R^4\rho\omega, u\right\} \\ &\quad -R\nabla\cdot\left[R^2\nabla_{pol}u\nabla\cdot\left(\rho\mathbf{v}\right)\right]+\left\{\psi, j\right\} \\ &\quad -\frac{F_0}{R}\frac{\partial j}{\partial\phi}+\left\{P, R^2\right\}+R\mu_\perp\left(T_e\right)\nabla^2_{pol}\omega, \end{aligned} \tag{14}$$

$$\omega = \frac{1}{R}\frac{\partial}{\partial R}\left(R\frac{\partial u}{\partial R}\right)+\frac{\partial^2 u}{\partial Z^2}, \tag{15}$$

$$\begin{aligned} B^2\frac{\partial}{\partial t}\left(\rho v_\parallel\right) &= -\frac{1}{2}\rho\frac{F_0}{R^2}\frac{\partial}{\partial\phi}\left(v_\parallel B\right)^2-\frac{\rho}{2R}\left\{B^2v_\parallel^2, \psi\right\}-\frac{F_0}{R^2}\frac{\partial P}{\partial\phi} \\ &\quad +\frac{1}{R}\left\{\psi, P\right\}-B^2\nabla\cdot\left(\rho\mathbf{v}\right)v_\parallel+B^2\mu_\parallel\nabla^2_{pol}v_\parallel. \end{aligned} \tag{16}$$

The vorticity equation Eq. (14) is obtained by applying $\nabla\phi\cdot\nabla\times\left(R^2\cdots\right)$ on both sides of the momentum equation.

The governing equations

Last, we write down the pressure equation for the single and the two temperature model separately. For the single temperature model,

$$\begin{aligned}\frac{\partial P}{\partial t} = & -\mathbf{v}\cdot\nabla P-\gamma P\nabla\cdot\mathbf{v}+\frac{\gamma-1}{R^2}\eta\left(T_e\right)j^2+\nabla\cdot\left(\kappa_\perp\nabla_\perp T+\kappa_\parallel\nabla_\parallel T\right)\\ & +\left(\gamma-1\right)\mu_\parallel\left[\nabla_{pol}\left(v_\parallel B\right)\right]^2-\left(\gamma-1\right)\left(P_{rad}+P_{ion}\right)\\ & +\frac{\gamma-1}{2}\mathbf{v}\cdot\mathbf{v}\left(S_{bg}+S_{imp}\right).\end{aligned} \tag{17}$$

Here, P_{rad} is the projected radiative power. The ionization power is defined by $P_{ion}\equiv\Delta E_{ion}/\Delta t$, where ΔE_{ion} is the projected ionization energy loss during the fluid time step Δt.

The governing equations

For the two temperature model, the equations are:

$$\begin{aligned}\frac{\partial}{\partial t}P_i &= -\mathbf{v}\cdot\nabla P_i - \gamma P_i \nabla\cdot\mathbf{v} + \nabla\cdot\left(\kappa_\perp \nabla_\perp T_i + \kappa_{i,\parallel}\nabla_\parallel T_i\right) \\ &\quad + \frac{\gamma-1}{2}\mathbf{v}\cdot\mathbf{v}\left(S_{bg}+S_{imp}\right) + (\gamma-1)\,\mu_\parallel\left[\nabla_{pol}\left(v_\parallel B\right)\right]^2 \\ &\quad + \left(n_{bg}+n_{imp}\right)\left(\partial_t T_i\right)_{c,e}, \end{aligned} \tag{18}$$

$$\begin{aligned}\frac{\partial}{\partial t}P_e &= -\mathbf{v}\cdot\nabla P_e - \gamma P_e \nabla\cdot\mathbf{v} + \nabla\cdot\left(\kappa_\perp \nabla_\perp T_e + \kappa_{e,\parallel}\nabla_\parallel T_e\right) \\ &\quad + \frac{\gamma-1}{R^2}\eta\left(T_e\right)j^2 - (\gamma-1)\left(P_{rad}+P_{ion}\right) + n_e\left(\partial_t T_e\right)_{c,i} \end{aligned} \tag{19}$$

The additional thermalization terms $\left(n_{bg}+n_{imp}\right)\left(\partial_t T_i\right)_{c,e}$ and $n_e\left(\partial_t T_e\right)_{c,i}$ are also dependent on the projected effective charge since the collisional ion-electron thermalization rate is proportional to the charge number squared of the ion species.

Fluid and particle impurity density

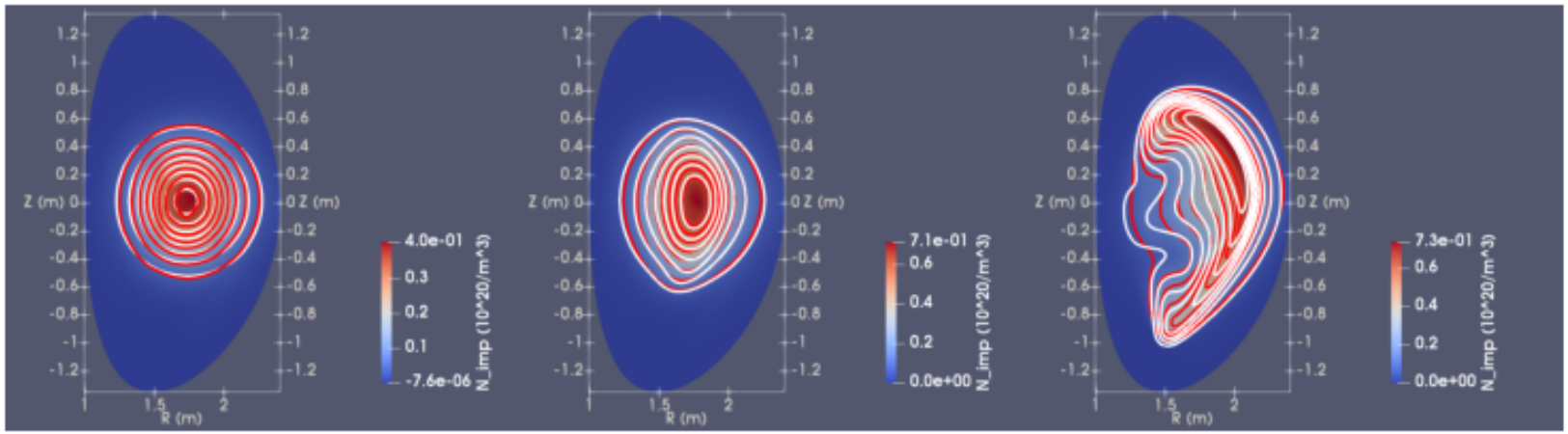

Figure 5. The impurity density contour comparison between the fluid description (white contours) and the particle moment projection (red contours) at (a) $t = 0.45ms$, (b) $t = 0.78ms$ and (c) $t = 1.10ms$. Note that the contours from each color are on exactly the same scale, so that matching contour lines indicate quantitative match of the two representations.

CE particle vs. fluid

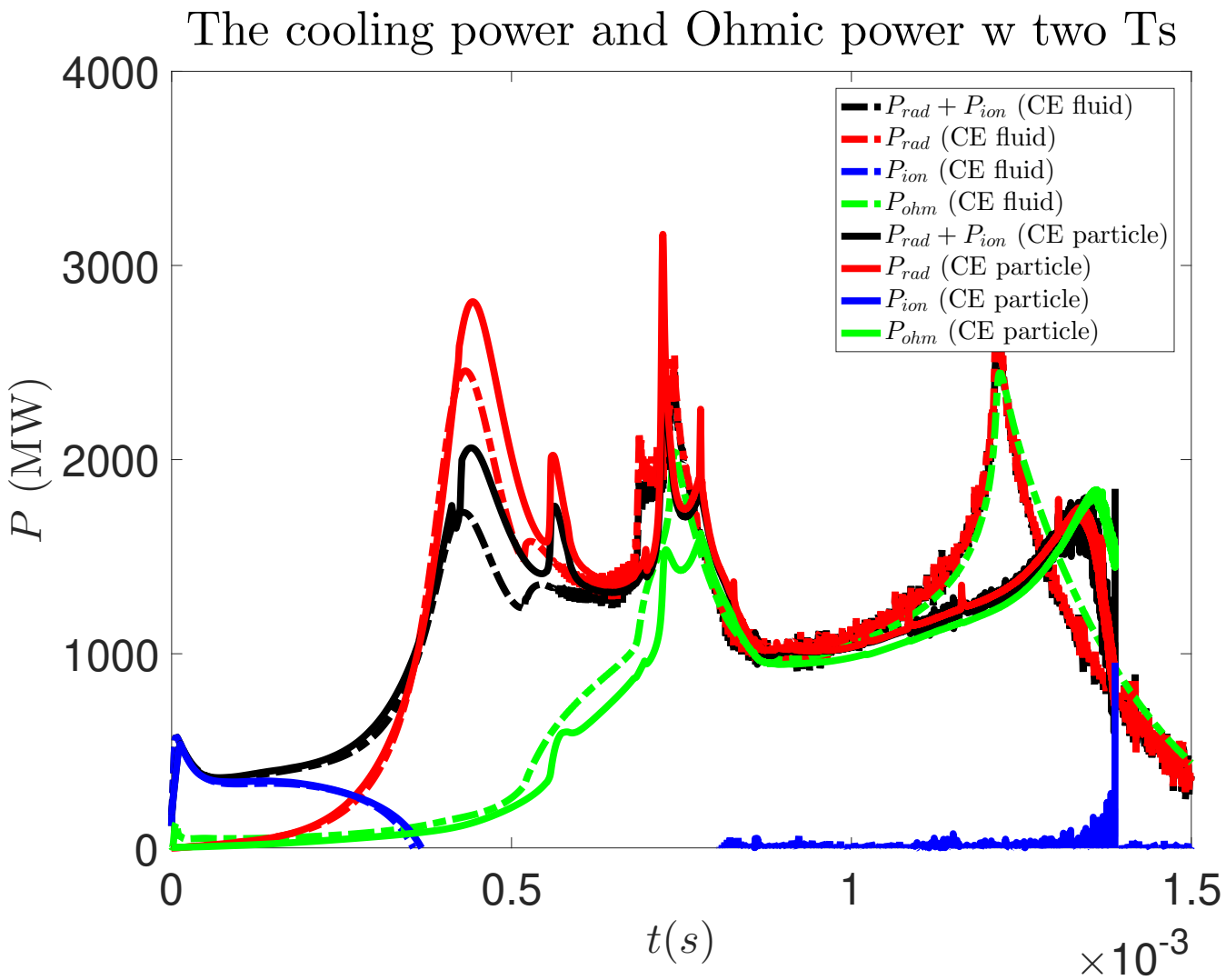

1942 ADAS data

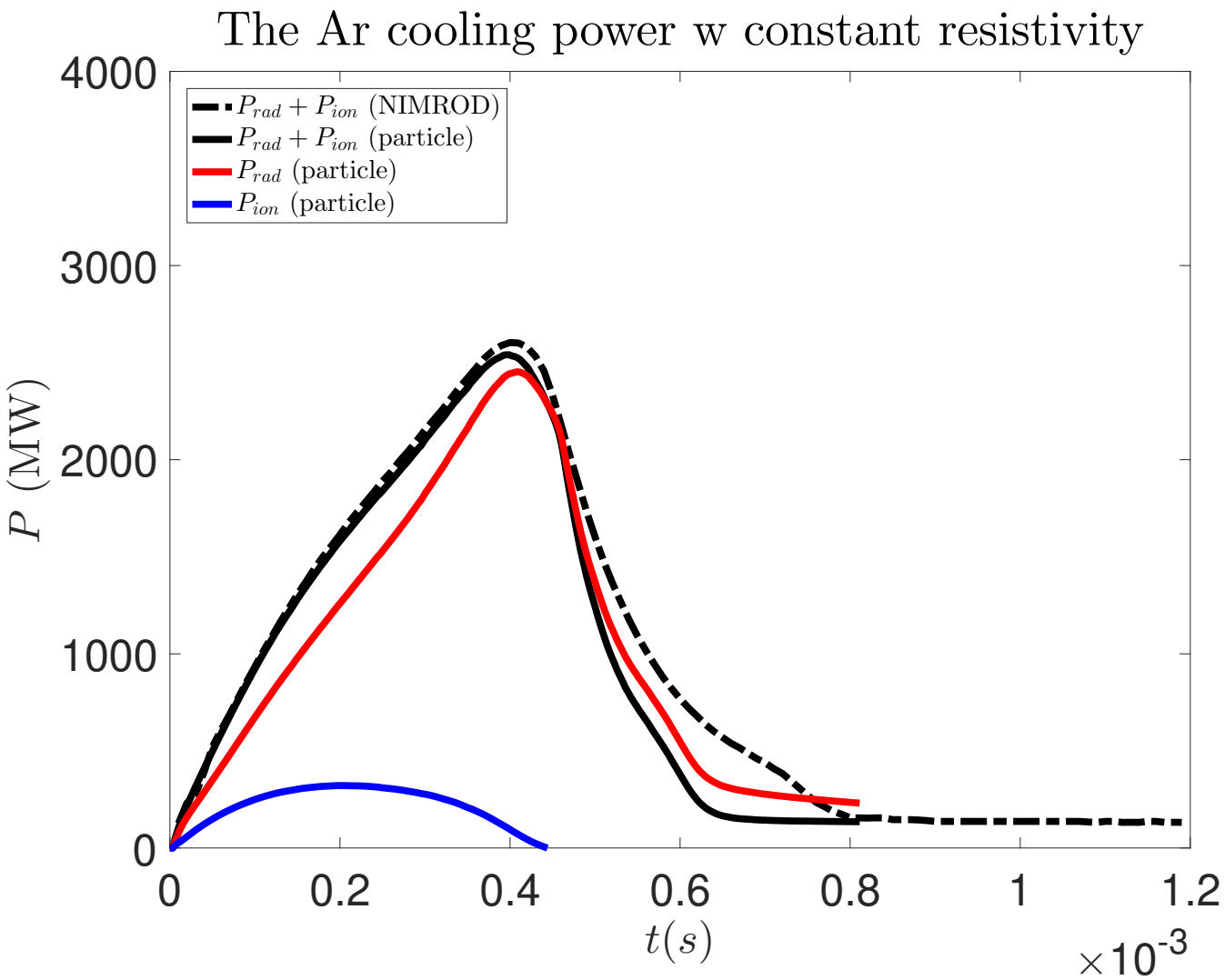

ADAS vs. KPRAD